Scanning Kerr microscopy study of current-induced switching in Ta/CoFeB/MgO films with perpendicular magnetic anisotropy

C. J. Durrant and R. J. Hicken
Department of Physics and Astronomy, University of Exeter, Exeter EX4 4QL, United Kingdom

Qiang Hao and Gang Xiao
Department of Physics, Brown University, Providence, Rhode Island 02912, USA

(Received 12 August 2015; revised manuscript received 8 December 2015; published 11 January 2016)

Ta/CoFeB/MgO trilayers with perpendicular magnetic anisotropy are expected to play a key role in the next generation of current and electric field switched memory and logic devices. In this study, we combine scanning Kerr microscopy with electrical transport measurements to gain insight into the underlying mechanisms of current-induced switching within such devices. We find switching to be a stochastic, domain-wall-driven process, the speed of which is strongly dependent on the switching current. Kerr imaging shows domain nucleation at one edge of the device, which modeling reveals is likely assisted by the out-of-plane component of the Oersted field. Further domain growth, leading to magnetization reversal, may still be dominated by spin torques, but the Oersted field provides an additional mechanism with which to control the switching process.

DOI: 10.1103/PhysRevB.93.014414

I. INTRODUCTION

The ever growing demand for higher density and faster processing speeds has led to great advances in the field of data storage in the past few decades [1]. The discovery of tunneling magnetoresistance (TMR) [2] has made the magnetic tunnel junction (MTJ) one of the leading candidates for next-generation high-density magnetic random access memory (MRAM) [3].

Existing MRAM requires an external magnetic field, generated by a current, to induce switching during the read/write procedure. Recently, there has been great interest in switching the memory bit directly by using spin-transfer torques (STT) generated by charge currents [4,5]. Conventional STT switching requires current to be injected directly through a tunnel barrier. However, recent studies have utilized the torques generated by spin Hall and Rashba effects to switch elements with an in-plane current, leading to smaller write currents for equivalent thermal stability, and avoiding degradation associated with passing high current densities through a tunnel barrier [6]. To date, these phenomena have been investigated mostly in layered structures containing HM/FM/Ox subunits in which the ferromagnetic (FM) layer is sandwiched between a heavy metal (HM) and an oxide (Ox) [7–13]. Spin-transfer torque magnetic random-access memory (STT-MRAM) has been explored as a replacement for dynamic random access memory (DRAM) and may provide performance comparable to DRAM main memory with an average 60% reduction in main memory energy [14]. With main memory energy now accounting for as much as 30% of overall system power [15,16], STT-MRAM has the potential to significantly reduce the operational cost of computing systems.

It has been demonstrated that the Ta/CoFeB/MgO subunit could fulfill the three criteria required for high-performance MTJs for STT-MRAM, namely high tunneling magnetoresistance (TMR), low switching current, and high thermal stability for small device dimensions. With TMR ratios of 120% in Ta/MgO/CoFeB/MgO/CoFeB/Ta [17] stacks and 162% in similar stacks with Mo layers [18], switching currents of (3–6) $\times$ 10^6 A/cm^2 for similar devices [19,20], and good thermal stability for devices with 40 nm diameter [17], Ta/CoFeB/MgO is indeed a viable candidate for next-generation STT-MRAM.

A deeper understanding of the underlying switching mechanisms is critical for effective device fabrication, and it has recently been the subject of much debate. Kim *et al.* [10] report a strong HM and FM thickness dependence of both the Rashba spin-orbit field and the spin Hall torques. Torrejon *et al.* [21] also report a strong thickness dependence of their relative contributions to the switching, with spin Hall torque dominating for thicker HM underlayers. The relative contributions made by these effects are also influenced by capping layer thickness [22] and temperature [19]. In this study, we combine scanning Kerr imaging with electrical transport measurements to gain further insight into the switching process. Crucially, current pulses of constant amplitude are applied so that the evolution of intermediate magnetic states can be probed under constant current conditions.

II. EXPERIMENT

A. Fabrication details

We focus only on CoFeB with the composition $Co_{40}Fe_{40}B_{20}$ in which perpendicular magnetic anisotropy (PMA) was achieved through thermal annealing. Stacks of Ta(4 nm)/CoFeB(1 nm)/MgO(1.6 nm)/Ta(1 nm) were sequentially deposited on thermally oxidized Si wafers in a high vacuum magnetron sputtering system. Further details of this process can be found in Ref. [23] . The 1 nm Ta layer was used as a capping layer to prevent atmospheric oxidization.

The stacks were patterned into 20 $\times$ 140 μm^2 Hall bars with 5-μm-wide contact pads [Fig. 1(d)] using photolithography. After stack deposition, a second round of photolithography and Au deposition was used to define contact pads. Au contacts were not critical for switching but allow wire-bonding to facilitate electrical measurements.

The sample was then annealed in vacuum (1 $\times$ 10^{-6} Torr) at 220 °C for 1 h with 2 h of ramping up and 6 h of natural cooling

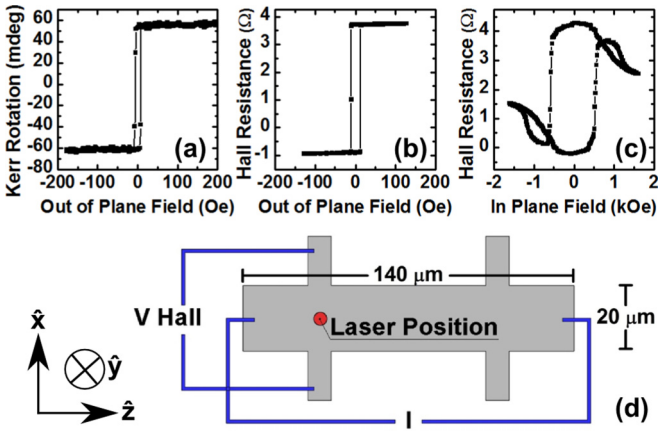

FIG. 1. Kerr rotation (a) measured midway between the contact pads as shown in (d), and Hall resistance (b) between the contact pads during sweeping of an out-of-plane ($\hat{\mathbf{y}}$) magnetic field. Part (c) shows the Hall resistance measured during sweeping of an in-plane magnetic field applied along the direction of the current ($\hat{\mathbf{z}}$).

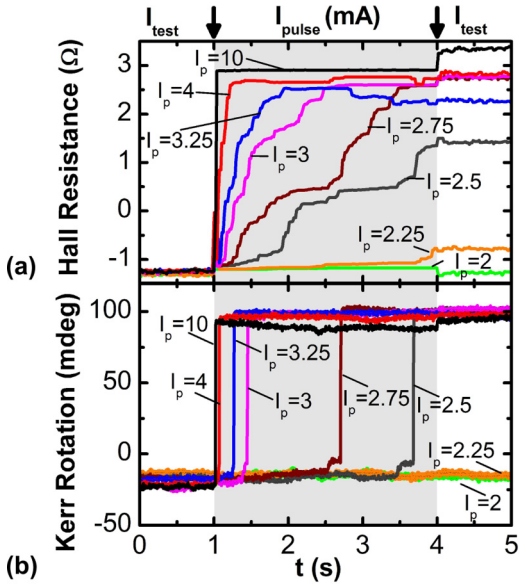

FIG. 2. Hall resistance (a) between the contact pads shown in Fig. 1(d) as the device undergoes magnetization switching induced by current pulses of 3 s duration with amplitude $I_p = 2.00$–10.00 mA, triggered at $t = 1$ s (darker background on graph). Hall resistance is measured using a current of 0.1 mA both before ($t = 0.0$–1.0 s) and after ($t = 4.0$–5.0 s) application of the pulse. Part (b) shows the simultaneous measurements of the Kerr rotation within a submicron region midway between the Hall contacts, also shown in Fig. 1(d).

under a magnetic field of 0.45 T perpendicular to the plane of the sample. It was shown by several groups [8,23,24] that the 220 °C annealing temperature is critical for the formation of robust PMA. As-prepared samples do not support PMA as they have sharp, but disordered, interfaces, while at high annealing temperatures (>220 °C) diffusion within the interfacial region is detrimental to the PMA.

B. Measurement details

For magnetotransport measurements, wire-bonding was used to connect the Hall bar to two 50 Ω coplanar waveguides (CPWs). A current was applied along the direction parallel to the long edge of the Hall bar ($\hat{\mathbf{z}}$), and the Hall resistance was measured across the contacts perpendicular to the current ($\hat{\mathbf{x}}$), as shown in Fig. 1(d). In this way, the magnetization between the contact pads was probed via the anomalous Hall effect (AHE). The Hall bar and CPWs were placed in a scanning Kerr microscope so that the magnetization within a submicron region could be probed via the magneto-optical Kerr effect (MOKE), simultaneously with the Hall resistance measurements. The MOKE measurement was performed by focusing the beam from a 633 nm He-Ne laser onto the sample surface with a 40× objective lens, and recording the optical rotation of the backreflected beam using a simple optical bridge detector. In each experiment, a large in plane field was used to set the initial perpendicular magnetization direction. The direction of the magnetization was reproducible due to a slight (<1°) tilt of the applied field relative to the plane of the Hall bar. The field was then reduced to remanence (≈7 Oe) along the direction of current flow, as shown in Fig. 1(c). All measurements were performed at room temperature.

III. RESULTS AND DISCUSSION

Using an out-of-plane ($\hat{\mathbf{y}}$) field, the saturation Kerr rotation [Fig. 1(a)] and Hall resistance [Fig. 1(b)] were found for each of the bistable out-of-plane magnetization $\mathbf{M}$ states. These results were used to confirm that full magnetization reversal had occurred in subsequent current-induced switching experiments. The devices showed a particularly low (≈10 Oe) perpendicular coercive field. The small difference in coercive field between Figs. 1(a) and 1(b) is likely due to the measurements being made at different times and therefore under slightly different conditions, e.g., the temperature in the laboratory may affect the coercivity given that the depinning of domain walls is thermally activated. The Hall resistance measured during the application of the in-plane field used to set the initial $\mathbf{M}$ state is shown in Fig. 1(c). The crossover observed at ±600 Oe is due to the <1° tilt of the field with respect to the sample plane.

A. Time-resolved–time-dependent current

In the magnetotransport measurements shown in Fig. 2(a), the initial magnetization state ($\mathbf{M}^-$) was measured with a small dc current $I_{\text{test}} = 0.10$ mA and found to correspond to a Hall resistance of −1.25 Ω. The magnetization was switched toward the opposite bistable state ($\mathbf{M}^+$), which corresponds to a Hall resistance of 3.25 Ω, by current pulses $I_p = 2.00$–10.00 mA with a duration of 3.0 s. I_{test} was then applied once more to measure the final magnetization state. Throughout this process, the Kerr rotation [Fig. 2(b)] was continuously monitored at a position midway between the Hall contacts shown in Fig. 1(d). The Hall resistance is expected to vary symmetrically about 0 Ω, and the 1 Ω offset is due to a slight misalignment of the Hall contacts. The longitudinal resistance of the bonded Hall bar was 2 kΩ, so a 1 Ω offset corresponds to a 0.05% longitudinal misalignment of the Hall contacts, which is within the tolerance of the photolithographic fabrication procedure.

For $I_p > 6.00$ mA, switching occurred on a time scale <1 μs, faster than the resolution of the measurement technique. By reducing the pulsed current to the range $I_p =$ 2.25–5.00 mA, switching occurs considerably more slowly, allowing the change in Hall resistance to be easily observed within the 3 s pulse duration. Due to the strong PMA, an intermediate Hall resistance value corresponds to a domain state in which the magnetization points either into or out of the plane. The intermediate Hall resistance is effectively equivalent to a line integral of all **M** states between the contact pads. This is confirmed by the Kerr rotation shown in Fig. 2(b), where the local **M** switches instantaneously between the two states. Switching in Fig. 2(b) coincides with large steps in the Hall resistance, which are most clear for currents in the range $I_p = 2.50$–4.00 mA. This implies that a large area (length equal to a few μm) switches simultaneously. Whether the switching is due to a single domain or a collection of smaller domains is difficult to determine, as for $I_p = 2.50$ and 2.75 mA a small step before full switching can be seen in the Kerr rotation [Fig. 2(b)]. This must be due to the full switching of a small domain, less than the size of the laser spot, or else the laser has been positioned on a domain wall at the upper edge of a larger domain.

For the highest currents [seen for $I_p = 10.00$ mA in Fig. 2(a)], the final Hall resistance is slightly larger than that observed for lower currents. This is likely due to the magnetization of the contact pad regions being more strongly pinned and requiring higher currents to switch than the body of the device. For higher currents (again seen clearly for $I_p = 10.00$ mA), the Hall resistance shows that full switching occurs within the first μs, but the final Hall resistance measured with I_{test} is larger than the Hall resistance measured during the pulse. This behavior may be due to the perpendicular component of the Oersted field (in the $\hat{\mathbf{y}}$ direction) opposing reversal on one edge of the device during I_p. This field will be significantly lower during I_{test}, when full reversal finally occurs. The role of the Oersted field will be discussed further in the final section of this paper.

For the lowest currents <2.25 mA, no switching occurs. The switching process is stochastic in nature, as shown in Fig. 3, and for repeated measurements switching was observed for a critical current of $I_c = 2.6 \pm 0.2$ mA, where the stated uncertainty indicates the full range of values for which complete switching was observed. Other studies have attributed the switching entirely to the giant spin Hall effect, and so they calculated critical current densities from the current in the Ta layer. Based on typical resistivities of $\rho_{\text{CoFeB}} =$ 100 $\mu\Omega$ cm and $\rho_{\text{Ta}} = 200$ $\mu\Omega$ cm [23], $\frac{2}{3}$ of the current is expected to flow through the Ta layer. This yields $I_c = 1.73 \pm$ 0.13 mA and a critical current density of $(2.16 \pm 0.16) \times 10^6$ A/cm^2. Although the critical parameter values are expected to depend upon both the temperature and the characteristic measurement time, the calculated critical current density is similar to values of (3–6) $\times 10^6$ A/cm^2 reported previously for the same material [19,20]. Indeed the critical current density is of comparable magnitude to the values reported for MTJs with in-plane anisotropy [25] and for giant magnetoresistance (GMR) spin-valve sensors [26].

The present experiment demonstrates the strong dependence of the switching speed on I_p. Care must therefore be taken when comparing with previous studies that have used different protocols to extract I_c. For example, the current may be swept at a given rate and the Hall voltage measured simultaneously. However, in this case, if the sweep rate is too high, details of intermediate states, such as those observed in Fig. 2(a) for $I_p = 2.5$ mA, may be lost and the critical current may be overestimated.

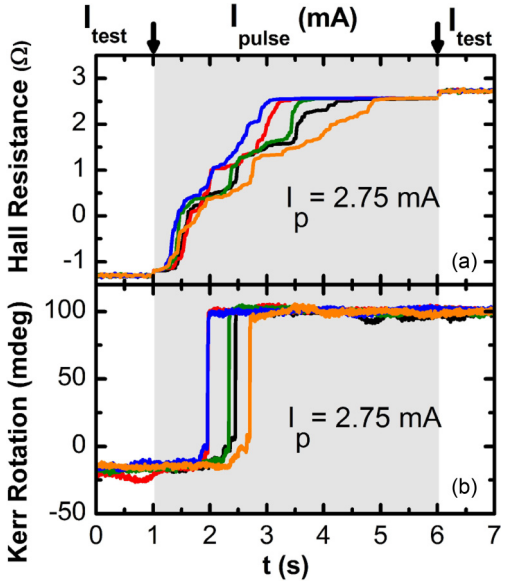

FIG. 3. Hall resistance (a) between the contact pads shown in Fig. 1(d) as the device undergoes five switching events under identical conditions induced by 5.0 s duration current pulses, with amplitude $I_p = 2.75$ mA, triggered at $t = 1.0$ s (darker background on graph). The Hall resistance is measured before ($t = 0.0$–1.0 s) and after ($t = 6.0$–7.0 s) the pulse using a current of 0.1 mA. Part (b) shows the simultaneous measurement of the Kerr rotation within a submicron region midway between the Hall contacts, also shown Fig. 1(d).

B. Time-resolved–constant current

During the experiments in which I_p was varied, the Hall resistance trace and the time of switching observed in the Kerr signal were not always the same for repeated switching measurements made with identical I_p. Figure 3 highlights the stochastic nature of this process showing five switching processes under nominally identical conditions for $I_p = 2.75$ mA. The parameters for this experiment were identical to those discussed for Fig. 2, but the pulse length was increased to 5.0 s so that full switching could be obtained within the duration of the pulse at a lower I_p value.

In the transport measurements shown in Fig. 3(a), the Hall resistance is similar in each event for the first 1.0 s of the pulse. The Hall resistance then diverges between 2.0 and 4.5 s before reaching the same saturation state in the final 4.5–6.0 s. The divergence coincides with a large step in the Hall resistance, which occurs at the same time as the large change in Kerr rotation seen in Fig. 3(b). As the Kerr rotation probes only the center of the device [Fig. 1(d)], it can be inferred that for the first 1.0 s of the pulse, domains at the edges of the Hall bar switch more easily than the magnetization at its center, and that switching follows a similar "path" in each event (the reasons

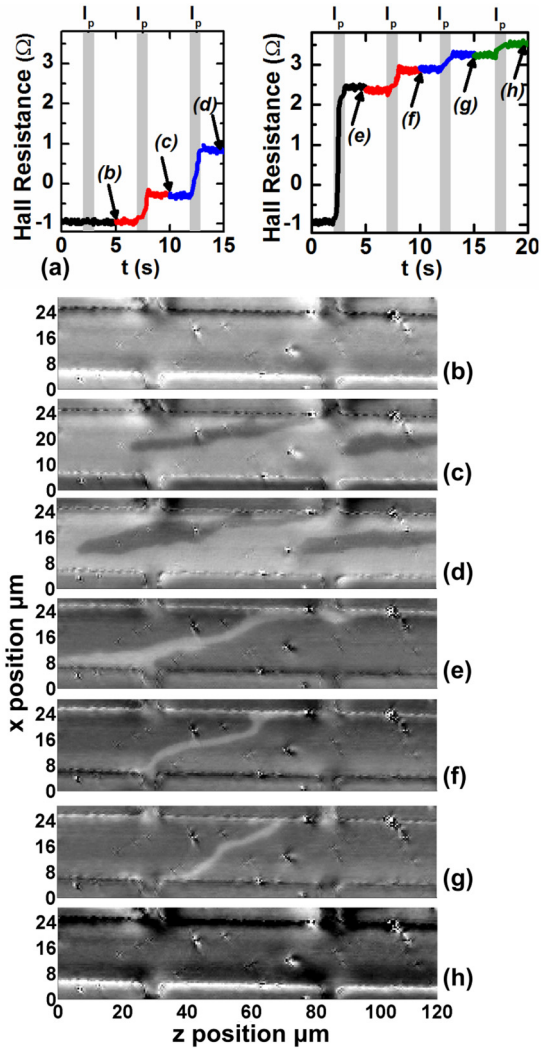

FIG. 4. (a) Hall resistance values between the contact pads shown in Fig. 1(d) for the magnetic domain state images shown in (b)–(h). The darker background in (a) indicates pulse on, while the lighter background indicates test current on.

for this will be discussed, and they are shown in Fig. 5). The switching of the central region, observed as a large step in Hall resistance and change in Kerr rotation, occurs later in the pulse and appears more random than the switching of the edge of the device.

C. Static imaging during current-induced switching

For further insight into the domain configuration during switching, scanning MOKE images were acquired for a series of stable (on the time scale of the imaging experiment) domain configurations during the switching process. Figure 4(a) shows the Hall resistance values at which the images (b)–(h) were taken. It was not feasible to image a single switching event, as the "mid" states (with **M** close to 50/50 in and out of plane) were unstable over the imaging time (several hours). Images were instead taken on either side of this unstable middle region for the two separate partial switching events shown in Fig. 4(a). Image (h) was subtracted from the remaining images to suppress topographic features and optimize the magnetic contrast. The strong dark and light contrast across the bottom of the bar in (h) may be associated with the incomplete removal of photoresist in that region.

Figure 4(b) shows $\mathbf{M}^-$ corresponding to a Hall resistance of $-1\ \Omega$. As I_p is applied, the formation (c) and growth (d) of large domains of $\mathbf{M}^+$ is observed. These domains appear to grow from the edge of the Hall bar and remain pinned at more than one site (e.g., $z = 60\ \mu$m, $x = 24\ \mu$m). For the second set of stable states, the majority of **M** lies in the $\mathbf{M}^+$ direction. The large reversed domain seen in (e) is in a similar position to the domain seen in (c) and (d) and also appears pinned at the same site. This domain then shrinks in (f) and (g) while remaining pinned until a full reversal to $\mathbf{M}^+$ is observed in (h).

To a first approximation, the Hall resistance should be proportional to the integral of the out-of-plane component of **M** evaluated along a line between the contact pads. The value of this integral can be compared to the percentage of reversed magnetization along the same line within the corresponding image. The minimum Hall resistance of $-1.25\ \Omega$ corresponds to 0% reversed magnetization while the maximum $3.25\ \Omega$ corresponds to 100%. The percentages of reversed magnetization inferred from the Hall resistance and Kerr images, respectively, are (c) 26% and 23%, (d) 39% and 41%, (e) 78% and 77%, (f) 88% and 87%, and (g) 96% and 95%. The magnetic states inferred by the two methods are therefore seen to be in excellent agreement.

Reverse domains appear to form first at the edge of the device for which $x = 24\ \mu$m, as observed in (b)–(d), and then they grow toward the center. When reversal is close to completion, the largest portion of the original domain state appears to be located on the opposite edge of the device, as seen clearly in (e) around $x = 4\ \mu$m. This may again be due to the presence of the Oersted field, with the $\hat{\mathbf{y}}$ component of this field (B_y) having peak magnitude but opposite polarity at the two long edges of the device.

D. Modeling the Oersted field

Many studies of similar structures do not discuss the presence of Oersted fields. Some studies [11,27] do calculate the in-plane component of the Oersted field (B_x) and conclude that it does not have any significant effect upon the switching since B_x is about one order of magnitude smaller than the effective fields generated by spin torques (Ref. [27] calculates 0.3 Oe/mA for a 20-μm-wide bar), and this field often acts to oppose the spin torques [7].

We demonstrate in the model shown in Fig. 5 that while B_x is indeed small, B_y can become comparable to the 10 Oe coercive field shown in Fig. 1, and so it may have a significant effect on the switching process, at least in the absence of an external field applied to the structure.

The Hall bar cross section ($20\ \mu$m $\times$ 4 nm Ta and 1 nm CoFeB) was modeled by filling it with wires of radius r, as shown in Fig. 5(a). The space in and around the bar was broken into a grid, and the field was calculated at each point from the Biot-Savart law.

A uniform current density was assumed in each layer. The current density in each layer was calculated assuming $\frac{2}{3}I$ in the Ta layer and $\frac{1}{3}I$ in the CoFeB (as discussed in the preceding

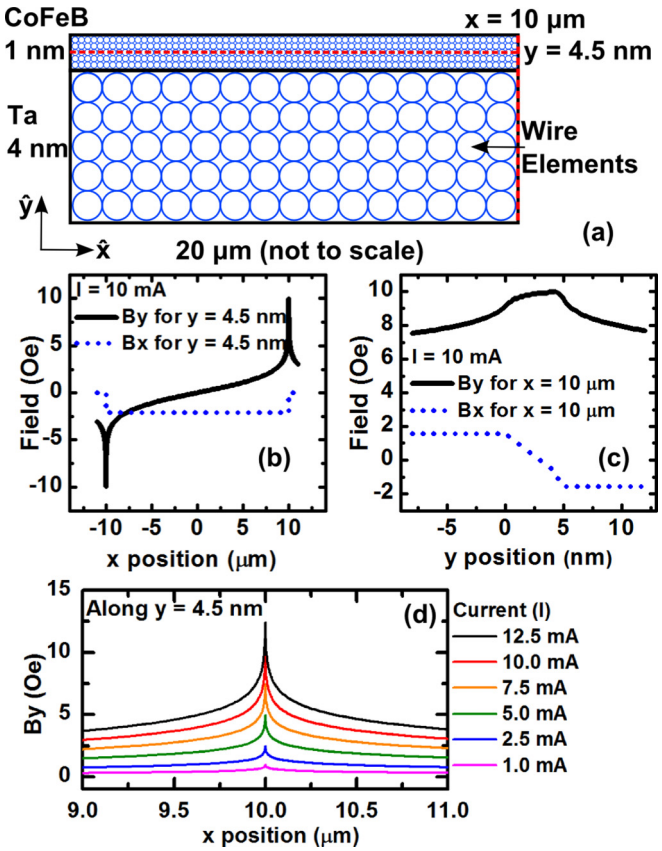

FIG. 5. Geometry (a) for calculation of Oersted fields in Ta/CoFeB layers modeled as an array of wire elements. Part (b) shows how the in-plane (B_x) and out-of-plane (B_y) components of the Oersted field vary across the width of the Hall bar along a line through the center of the CoFeB layer. Part (c) shows the variation of these fields across the thickness of the layers at the edge of the Hall bar where the out-of-plane field has maximum value. Part (d) shows how the out-of-plane field varies with current along a line through the center of the CoFeB layer close to the edge of the Hall bar.

section), and the current in an individual wire was adjusted to take account of the packing fraction. The current was assumed to flow perpendicular to the cross-sectional plane, shown in Fig. 5(a) in the $\hat{\mathbf{z}}$ direction. Each layer was assumed to have a thickness equivalent to five wire diameters ($r_{\mathrm{CoFeB}} = 1/10$ nm and $r_{\mathrm{Ta}} = 4/10$ nm) in order to optimize computation time. A further increase in the number of wires contained within the layer made a negligible difference to the calculated field.

In Fig. 5, the $\hat{\mathbf{x}}$ direction has again been defined along the width of the Hall bar (20 μm) while $\hat{\mathbf{y}}$ lies perpendicular to the plane. Figure 5(b) shows B_y and B_x along a line through the center of the CoFeB layer at $y = 4.5$ nm for $I_p = 10$ mA. The field profile is as expected for a current-carrying strip [28], and B_x is in good agreement with fields calculated in Ref. [27] . We observe a sharp peak in B_y with a height of about ± 10 Oe close to the edges of the bar. These fields are comparable to the 10 Oe out-of-plane coercive fields observed for this device in Fig. 1. The magnitude of the Oersted field varies little through the thickness of the CoFeB layer, as shown at the field peak around $x = 10$ μm in Fig. 5(c). These results, in conjunction with Fig. 4, may explain the domain behavior at the edges of the device. On one edge, B_y aids the reversal of domains, while on the opposite edge it opposes reversal. This effect may be lessened as I_p and hence B_y are reduced, as shown in Fig. 5(d). Even for $I_p = 5$ mA, the Oersted field is still about 50% of the coercive field, and so it is still likely to influence the switching process.

With recent interest in resolving the contributions of several mechanisms to the switching of similar devices, this result shows that Oersted fields may not always be discounted when interpreting the relative contribution of each switching mechanism, and also that care must be taken when designing devices of this type. A simple method of minimizing B_y, so as to explore only the spin-torque contributions to the switching, is therefore to perform a postdeposition etch to remove CoFeB at the edges of the Hall bar, leaving only the Ta underlayer. In the majority of recent studies, the HM underlayer has been thicker than the FM layer, and so it carries the majority of current, meaning that perpendicular Oersted fields in the FM would be effectively minimized by this approach. Another approach to studying the spin-transfer torque is to apply an in-plane external magnetic field to the structure, so that switching occurs via coherent rotation [23] of magnetization rather than by domain nucleation and growth.

IV. SUMMARY

Current-induced switching in perpendicularly magnetized Ta/CoFeB/MgO layers was studied by simultaneous Kerr microscopy and electrical transport measurements, focusing on currents close to the critical value for switching. For zero applied magnetic field, we find the switching to be a stochastic domain-wall-driven process, the speed of which is strongly dependent upon the value of the applied current. The nucleation of reverse domains appears to begin at one edge of the device before these domains then grow toward the center of the Hall bar. Modeling the Oersted field through the cross section of the Hall bar reveals that the out-of-plane component is comparable to the 10 Oe out-of-plane coercive field of the CoFeB, suggesting that the Oersted field may assist the initial domain nucleation on one edge of the Hall bar while opposing reversal on the other edge.

With recent interest in utilizing Ta/CoFeB/MgO layers in perpendicular magnetic tunnel junctions, this study highlights the need for careful consideration of the Oersted field when analyzing potential contributions to the switching process. Minimization of the Oersted field contribution, to facilitate the study of spin torques, can be achieved by etching the CoFeB layer at the edge of the device, although it may also be possible to utilize these fields to improve switching efficiency in future technologies.

ACKNOWLEDGMENTS

The authors wish to thank Tom Loughran, Rob Valkass, Paul Keatley, Wenzhe Chen, and Shu-tong Wang for assistance and discussion. This work was supported by the University of Exeter through the award of a scholarship to C.J.D., and at Brown University by the Nanoelectronics Research Initiative (NRI) through the Institute for Nanoelectronics Discovery and Exploration (INDEX), and by the National Science Foundation through Grant No. DMR-1307056.

[1] Z. Z. Bandic and R. H. Victora, Advances in magnetic data storage technologies, Proc. IEEE **96**, 1749 (2008).

[2] M. Julliere, Tunneling between ferromagnetic films, Phys. Lett. A **54**, 225 (1975).

[3] K. Ando, S. Fujita, J. Ito, S. Yuasa, Y. Suzuki, Y. Nakatani, T. Miyazaki, and H. Yoda, Spin-transfer torque magnetoresistive random-access memory technologies for normally off computing (invited), J. Appl. Phys. **115**, 172607 (2014).

[4] J. C. Slonczewski, Current-driven excitation of magnetic multilayers, J. Magn. Magn. Mater. **159**, L1 (1996).

[5] L. Berger, Emission of spin waves by a magnetic multilayer traversed by a current, Phys. Rev. B **54**, 9353 (1996).

[6] A. Driskill-Smith, D. Apalkov, V. Nikitin, X. Tang, S. Watts, D. Lottis, K. Moon, A. Khvalkovskiy, R. Kawakami, X. Luo, A. Ong, E. Chen, and M. Krounbi, *Latest Advances and Roadmap for In-Plane and Perpendicular STT-RAM*, in *3rd IEEE International Memory Workshop (IMW)* (IEEE, Piscataway, NJ, 2011), pp. 1–3.

[7] L. Liu, C.-F. Pai, Y. Li, H. W. Tseng, D. C. Ralph, and R. A. Buhrman, Spin-torque switching with the giant spin Hall effect of tantalum, Science (NY) **336**, 555 (2012).

[8] C. O. Avci, K. Garello, C. Nistor, S. Godey, B. Ballesteros, A. Mugarza, A. Barla, M. Valvidares, E. Pellegrin, A. Ghosh, I. M. Miron, O. Boulle, S. Auffret, G. Gaudin, and P. Gambardella, Fieldlike and antidamping spin-orbit torques in as-grown and annealed Ta/CoFeB/MgO layers, Phys. Rev. B **89**, 214419 (2014).

[9] K. Garello, I. M. Miron, C. O. Avci, F. Freimuth, Y. Mokrousov, S. Blügel, S. Auffret, O. Boulle, G. Gaudin, and P. Gambardella, Symmetry and magnitude of spin-orbit torques in ferromagnetic heterostructures, Nat. Nanotechnol. **8**, 587 (2013).

[10] J. Kim, J. Sinha, M. Hayashi, M. Yamanouchi, S. Fukami, T. Suzuki, S. Mitani, and H. Ohno, Layer thickness dependence of the current-induced effective field vector in Ta/CoFeB/MgO, Nat. Mater. **12**, 240 (2013).

[11] G. Yu, P. Upadhyaya, Y. Fan, J. G. Alzate, W. Jiang, K. L. Wong, S. Takei, S. A. Bender, L.-T. Chang, Y. Jiang, M. Lang, J. Tang, Y. Wang, Y. Tserkovnyak, P. K. Amiri, and K. L. Wang, Switching of perpendicular magnetization by spin-orbit torques in the absence of external magnetic fields, Nat. Nanotechnol. **9**, 548 (2014).

[12] G. Yu, P. Upadhyaya, K. L. Wong, W. Jiang, J. G. Alzate, J. Tang, P. K. Amiri, and K. L. Wang, Magnetization switching through spin-Hall-effect-induced chiral domain wall propagation, Phys. Rev. B **89**, 104421 (2014).

[13] T. Suzuki, S. Fukami, N. Ishiwata, M. Yamanouchi, S. Ikeda, N. Kasai, and H. Ohno, Current-induced effective field in perpendicularly magnetized Ta/CoFeB/MgO wire, Appl. Phys. Lett. **98**, 142505 (2011).

[14] E. Kultursay, M. Kandemir, A. Sivasubramaniam, and O. Mutlu, *Evaluating STT-RAM as an Energy-efficient Main Memory Alternative*, in *2013 IEEE International Symposium on Performance Analysis of Systems and Software (ISPASS)* (IEEE, Piscataway, NJ, 2013), pp. 256–267.

[15] J. Carter and K. Rajamani, Designing energy-efficient servers and data centers, Computer **43**, 76 (2010).

[16] U. Hoelzle and L. A. Barroso, *The Datacenter as a Computer: An Introduction to the Design of Warehouse-Scale Machines* (Morgan and Claypool Publishers, 2009).

[17] S. Ikeda, K. Miura, H. Yamamoto, K. Mizunuma, H. D. Gan, M. Endo, S. Kanai, J. Hayakawa, F. Matsukura, and H. Ohno, A perpendicular-anisotropy CoFeB-MgO magnetic tunnel junction, Nat. Mater. **9**, 721 (2010).

[18] H. Almasi, D. Reifsnyder Hickey, T. Newhouse-Illige, M. Xu, M. R. Rosales, S. Nahar, J. T. Held, K. A. Mkhoyan, and W. G. Wang, Enhanced tunneling magnetoresistance and perpendicular magnetic anisotropy in Mo/CoFeB/MgO magnetic tunnel junctions, Appl. Phys. Lett. **106**, 182406 (2015).

[19] X. Qiu, P. Deorani, K. Narayanapillai, K.-S. Lee, K.-J. Lee, H.-W. Lee, and H. Yang, Angular and temperature dependence of current induced spin-orbit effective fields in Ta/CoFeB/MgO nanowires, Sci. Rep. **4**, 4491 (2014).

[20] C. Zhang, M. Yamanouchi, H. Sato, S. Fukami, S. Ikeda, F. Matsukura, and H. Ohno, Magnetization reversal induced by in-plane current in Ta/CoFeB/MgO structures with perpendicular magnetic easy axis, J. Appl. Phys. **115**, 17C714 (2014).

[21] J. Torrejon, F. Garcia-Sanchez, T. Taniguchi, J. Sinha, S. Mitani, J.-V. Kim, and M. Hayashi, Current-driven asymmetric magnetization switching in perpendicularly magnetized CoFeB/MgO heterostructures, Phys. Rev. B **91**, 214434 (2015).

[22] X. Qiu, K. Narayanapillai, Y. Wu, P. Deorani, D.-H. Yang, W.-S. Noh, J.-H. Park, K.-J. Lee, H.-W. Lee, and H. Yang, Spin-orbit-torque engineering via oxygen manipulation, Nat. Nanotechnol. **10**, 333 (2015).

[23] Q. Hao and G. Xiao, Giant spin Hall effect and magnetotransport in a Ta/CoFeB/MgO layered structure: A temperature dependence study, Phys. Rev. B **91**, 224413 (2015).

[24] D. C. Worledge, G. Hu, D. W. Abraham, J. Z. Sun, P. L. Trouilloud, J. Nowak, S. Brown, M. C. Gaidis, E. J. O'Sullivan, and R. P. Robertazzi, Spin torque switching of perpendicular Ta/CoFeB/MgO-based magnetic tunnel junctions, Appl. Phys. Lett. **98**, 022501 (2011).

[25] S. Ikeda, J. Hayakawa, Y. M. Lee, F. Matsukura, Y. Ohno, T. Hanyu, and H. Ohno, Magnetic tunnel junctions for spintronic memories and beyond, IEEE Trans. Electron Dev. **54**, 991 (2007).

[26] D. Lacour, J. A. Katine, N. Smith, M. J. Carey, and J. R. Childress, Thermal effects on the magnetic-field dependence of spin-transfer-induced magnetization reversal, Appl. Phys. Lett. **85**, 4681 (2004).

[27] L. Liu, O. J. Lee, T. J. Gudmundsen, D. C. Ralph, and R. A. Buhrman, Current-Induced Switching of Perpendicularly Magnetized Magnetic Layers Using Spin Torque from the Spin Hall Effect, Phys. Rev. Lett. **109**, 096602 (2012).

[28] P. S. Keatley, V. V. Kruglyak, A. Neudert, E. A. Galaktionov, R. J. Hicken, J. R. Childress, and J. A. Katine, Time-resolved investigation of magnetization dynamics of arrays of nonellipsoidal nanomagnets with nonuniform ground states, Phys. Rev. B **78**, 214412 (2008).